ARTICLE INFO
Article ID: 01-13-02-0020

doi:10.4271/01-13-02-0020

Particle Swarm Optimization with Required Time of Arrival Constraint for Aircraft Trajectory

Alejandro Murrieta-Mendoza,[1] Ruxandra Mihaela Botez,[1] Hugo Ruiz,[1] and Sonya Kessaci[1]

[1]École de Technologie Supérieure/Université du Québec, Canada

Abstract

Global warming has motivated the aeronautical industry to develop new technologies that will reduce polluting emissions. A direct way to achieve this goal is to reduce fuel consumption. Reference trajectory optimization contributes to this goal by guiding aircraft to zones where meteorological conditions are favorable to execute their required missions and thereby to reduce flight costs. In this article, the reference trajectory was optimized in terms of geographical position, altitude, and speed, by taking into account a Required Time of Arrival (RTA) constraint and weather conditions. The algorithm assumes that there is no traffic and that the aircraft can fly anywhere in the search space. The search space was modeled in the form of a unidirectional weighted graph, fuel burn was computed using a numerical model, and the weather forecast was taken into account. The methodology utilized in this article to determine the most economical combinations of parameters that delivered the optimal trajectory was inspired by the Particle Swarm Optimization (PSO) algorithm. Results showed that the algorithm provided acceptable solutions under traffic management constraints. It was observed that the developed algorithm was able to save up to 9.1% (6,800 kg) of fuel burn when there was no RTA constraint for flight trajectories and up to 1.8% (600 kg) of fuel against real, as-flown trajectories with an RTA constraint of ±30 seconds. Because of the nature of the PSO Algorithm, the local best trajectories are extracted and provided as a Trajectory Option Set (TOS), which is similar in cost as the optimal trajectory.

History

Received: 03 Jun 2020
Revised: 24 Sep 2020
Accepted: 09 Nov 2020
e-Available: 20 Nov 2020

Keywords

Optimization, Commercial Aircraft, Trajectory, 4D, Particle Swarm Optimization, Fuel Burn, Emissions, Algorithm, Metaheuristics, Weather

Citation

Murrieta-Mendoza, A., Botez, R., Ruiz, H., and Kessaci, S., “Particle Swarm Optimization with Required Time of Arrival Constraint for Aircraft Trajectory,” *SAE Int. J. Aerosp.* 13(2):269-291, 2020, doi:10.4271/01-13-02-0020.

ISSN: 1946-3855
e-ISSN: 1946-3901

This article is part of a Special Issue on Innovations for Sustainable Aviation.

Introduction

Global warming has become paramount to many different organizations due to its severe impact on the environment. The use of fossil fuels has been identified as a significant cause of global warming due to their polluting particles released when these fuels are burned. These particles include, among others, carbon dioxide (CO_2), nitrogen oxides (NOx), hydrocarbons, and sulfur. Not all of these particles cause global warming; some of them lead to other harmful effects such as NOx and ozone-layer depletion, sulfur could damage vegetation and have a direct negative impact on human health such as the case of hydrocarbons and sulfur [1, 2].

The global tendency, therefore, is to reduce the quantity of fuel required to execute a given task. This tendency has not been gone unnoticed in the aeronautical industry, as burning fuel is necessary to power flights. The aeronautical industry has set itself multiple environmental goals. After having achieved significant reductions in NOx, the aeronautical industry is actively working to meet its goal of reducing CO_2 emissions by 2050 to 50% of those recorded in 2005 [3, 4], a direct way to reduce emissions as regards to reducing the fuel quantity required for the aircraft to fly a given distance. Requirements for CO_2 levels reduction have already begun to change the conventional wind patterns, making some round-trips longer and, thus, more expensive, as evaluated in [5].

Several technologies such as engine improvements, state-of-the-art aerodynamics, and weight reduction, as well as the use of alternative fuels such as biofuels, have been successfully implemented to reduce polluting emissions. These technologies are becoming more and more available on new aircraft; they can also be implemented in older aircraft but would require costly structural modifications. However, because the new generation of aircraft by itself will not be able to attain the pollution reduction goals [6], more alternatives are required.

However, simple operational procedures, such as engine washing, reduction of the APU use, gate electrical power, and assisted taxiing, among others, could have an impact on fuel consumption reduction [7]. Improving traffic efficiency is also a way to reduce fuel burn by allowing aircraft to minimize the time spent on the ground with engines functioning.

The most fuel burn porting occurs when an aircraft is airborne. Improving the reference trajectory for descents has been proven to reduce fuel burn and emissions. This reduction was attained by following the procedure called Continuous Descent Approach (CDA) [8]. Under this concept, an aircraft descends with engines in IDLE. Reducing fuel consumption during the descent phase is especially worthwhile, as it reduces the amount of released polluting particles near populated areas. Algorithms suggesting the optimal aircraft sequencing to merge to the runway following the CDA, and fulfilling the RTA constraint were developed in [9, 10]. Certain procedures, such as the missed approach, should be avoided as much as possible because they lead to the release of higher quantities of pollution close to heavily populated areas [11, 12].

While descent is a relevant phase for long-haul flights in terms of fuel burn, for this type of flight, the cruise is the phase that requires the most fuel burn. Therefore, besides making the aircraft flight at its optimal altitude and speeds, guiding aircraft to places in the atmosphere where weather patterns and conditions are favorable for the aircraft enables the opportunity to obtain noticeable fuel reductions. However, different studies in the United States and Turkey have shown that aircraft do not do this as they fly at their optimal speeds and altitudes [13, 14, 15]. This situation can be attributed to traffic, airline policies, and/or a lack of traffic management capabilities.

Before takeoff, each aircraft should deliver a flight plan to the Air Traffic Management (ATM) so that the required flight preparations are considered to accommodate it. Once an aircraft is in the air, Air Traffic Control (ATC) is responsible for flight safety by guaranteeing enough separation between aircraft. Any changes in the flight plan required by the crew should be authorized by the ATC. These changes include, among others, any change of altitude, change of heading, change of airport, etc. [16].

The flight plan consists of a set of waypoints using the earth as reference (ground track or lateral reference trajectory) that an aircraft should follow from the initial to the destination airport. Each waypoint should be attained by the aircraft at a certain speed and altitude (vertical reference trajectory). Thus reference trajectory optimization consists mostly of delivering the most economical flight plan (either before or while airborne).

These conventional trajectories have been optimized in the literature using different algorithms. Lidén, one of the pioneers of trajectory optimization, studied flight trajectory optimization [17] and the winds' effects on their flight cost [18]. Singular optimal control was applied in [19] to find the constant altitude, the speed variation, and the throttle setting that minimized fuel burn. Rosenow et al. [20] developed an algorithm that optimized the lateral reference trajectory (LNAV) following a series of waypoints. Dhief et al. [21] have evaluated two different algorithms that are able to generate optimal conflict-free trajectories over the North Atlantic airspace, intending to propose an alternative to the organized tracking system. The most economical constant altitude for the cruise phase using a fuel burn estimator was determined using the algorithm developed in [22]. Algorithms following ATC-desired flight trajectory constraints, such as constant segment altitudes and constant speed, have also been developed: Based on heuristics and parametric optimization, an algorithm was developed to study the effects of restricting the altitudes and speeds to discrete values [23]. In another algorithm, the most economical altitude for a short flight was computed using the Golden-Section Search algorithm, and an exhaustive search was implemented to find the most economical waypoints needed to change altitudes during cruise [24]. A beam search algorithm was implemented in [25] to find the most economical combination of speeds and altitudes as a means to reduce the flight cost. This algorithm was improved in [26] by adding a search space reduction technique and combined the beam search method, providing optimal or really good suboptimal solutions in a fraction of the time [27]. Using a precomputed Mach number database, Dijkstra's algorithm was used to find the most convenient waypoints to execute a step climb [28]. Sidibe and Botez [29] proposed a dynamic programming algorithm to compute the optimal vertical reference trajectory (VNAV), while Genetic Algorithms (GAs) have been used in [30] to find the most economical waypoints to execute step climbs.

However, as airspace is reaching its operational limits, ATM is improving airspace flexibility to allow what is called *Trajectory-Based Operations*. Under this concept, the aircraft would be free to fly on any trajectory within the airspace while in negotiation with ATC and other aircraft. This is of special interest to the Federal Aviation Administration under the NextGen concept [31] and for the Single European Sky ATM Research (SESAR) initiative in Europe.[1] This operation allows the possibility of optimizing in three-dimensional (3D) (LNAV and VNAV) without having to follow a predefined flight plan, thus taking contrail formation into account. Contrails are water vapor formed under specific weather circumstances due to the engines' exhaust temperature. It is supposed that contrails may be more harmful than CO_2; however, more studies are required to confirm it. Mixed-Integer Optimal Control has been implemented to optimize an aircraft's reference trajectory by avoiding contrail formation [32, 33, 34, 35]. Avoiding contrail formation zones might have the drawback that fuel consumption could increase as those zones could be more fuel efficient.

Other algorithms searching for favorable wind conditions to reduce fuel burn at a fixed altitude have been developed using Dijkstra's algorithm [36], A* [37], Floyd-Warshall [38], GAs [39], Artificial Bee Colony (ABC) [40], and Artificial Ant Colony (ACO) [41]. An algorithm used for a general aircraft to avoid obstacles was implemented in [42]. Ng et al. determined the ground track and then the VNAV under the influence of winds in [43]. GAs were also implemented to find the 3D optimal trajectory by taking into account climb, cruise, and descent phases [44]. These algorithms were later improved to allow changes in Mach number to increase fuel savings [45]. Dijkstra's algorithm was also useful in determining the most economical combination of waypoints under the free-flight concept [46].

[1] https://www.sesarju.eu/news/sesar-ju-confirms-benefits-collaborative-trajectory-based-operations

It is expected that Unmanned Aerial Vehicles (UAVs) will be able to fly in the airspace during the forthcoming years. Research has also been done on UAVs, as shown in the case described in [47]; the Dead Reckoning and Kalman filter were used for the UAV trajectory tracking. The optimization of UAVs formation has also been of interest for different applications [48, 49].

The future ATM/ATC will require aircraft to arrive at a certain waypoint at a given time. This constraint is called the Required Time of Arrival (RTA), or 4D trajectory optimization algorithm. To solve it, one of the first algorithms was proposed by Lidén [50]. Then using dynamic programming-based optimization algorithms were proposed [51, 52]. The state-of-the-art literature uses metaheuristic algorithms. The ACO was used [53] to find the most economical combinations of Mach numbers that fulfill the RTA constraint. The ABC was used in [54] to find the most economical combination of waypoints in the VNAV, as well as the most economical combination of Mach numbers that fulfill the RTA constraint. Dai et al. [55] solved the 4D trajectory optimization problem by using simulated annealing while solving aircraft conflicts. Another aspect of the 4D trajectory optimization research consists of developing systems able to manage the negotiations between various aircraft [56, 57, 58].

The contribution of this paper is the development of an algorithm using the metaheuristic Particle Swarm Optimization (PSO) technique that finds the most economical trajectory while fulfilling the RTA constraint for a long-haul flight by taking into account weather information. This article as well aims to evaluate the potential fuel savings of the algorithm. The previous version of this algorithm was presented in [59] and [60], however, those were preliminary results that only evaluated the feasibility of the algorithm in reduced dimensions as only RTA and only VNAV and LNAV. The PSO was selected because it provides very good solutions to a large search space [61], as is the case in the reference trajectory optimization problem, it also consists of evaluating different solutions instead of solving mathematical equations such as in control-oriented algorithms or gradient-oriented algorithms. This algorithm has not yet been explored in the literature for the 4D commercial aircraft reference trajectory optimization problem under basic air traffic constraints such as constant altitude and constant Mach number segments. An additional advantage of using the PSO algorithm is that, due to its nature, it can provide Trajectory Option Sets (TOSs); the TOSs are the suboptimal trajectories developed by the PSO algorithm while solving for the optimal trajectory. TOSs have been of interest, as they are suboptimal trajectories that the aircraft could follow in case of disruption on its current optimal trajectory [62, 63]. The lateral and the vertical trajectories are obtained simultaneously by the algorithm instead of obtaining firstly the lateral trajectory and then the vertical trajectory. The developed algorithm does not take into account all aspects of operations. For example, it assumes that the airspace is free of traffic and that all the decisions such as changes of altitude or changes of heading are allowed, the aircraft is able to fly within all the airspace. This algorithm however takes into account typical constraints such as flying at 1,000 ft steps at a constant speed.

This article is organized as follows: the next section explains how the fuel burn and flight costs are calculated, the effect of weather models, and how this information is used to compute the overall flight cost. Section III gives the methodology followed to implement the PSO. Finally, the results and conclusions are presented and further evaluated in Section IV.

I. Fuel Burn and Weather Models

A. Flight Cost

Airlines compute flight costs by not only taking into account fuel burn but also different time-related costs such as the crew's salary, aircraft maintenance cycles, the cost of missing or arriving early or late to a given destination, and lost connections. A parameter called the Cost Index is used to translate time-related costs in terms of fuel burn. The flight cost can be computed by using Equation 1.

$$Flight\ Cost = Fuel\ Burn + Cost\ Index * Flight\ Time \qquad \text{Eq. (1)}$$

where *Flight Time* corresponds to the time required to complete the flight and *Fuel Burn* is the total fuel consumed to complete the flight. The *Cost Index* emphasizes either the flight time or the fuel burn; if the airline must save fuel (and reduce emissions), the *Cost Index* is set to values tending to 0, as *Flight Time* is not considered important. If the airline instead must arrive as early as possible to a given destination, the *Cost Index* is set at its highest value (typically 99 or 999); in this case, reducing *Fuel Burn* is not important.

B. Fuel Burn Model

The fuel burn is computed using a point mass numerical performance model. This model, created from flight experimental data and arranged in the form of a database, is similar to the one used by some commercial Flight Management Systems. This model consists of inputs that define the flight profile and outputs such as the fuel flow, fuel burn, or/and horizontal traveled distance. Since this article focuses on the cruise phase, only the information for the cruise and climb/descent in Mach are taken into account. This model can be graphically represented in Figure 1, where CG stands for the Center of Gravity.

The numerical performance model is arranged so that the inputs should be available to provide the required output. The altitudes and the Mach numbers' inputs will always be the exact values available in the numerical model (Mach number separated in 0.05 steps and altitude separated in 1,000 ft steps). However, gross weight and temperature will normally not be the values available in the numerical performance model. The reason is that the gross weight diminishes as fuel is burned, and the temperature is a completely random value dependent upon the weather.

Linear interpolations are required to compute the required outputs. The interpolation sequence and special considerations required to compute the flight cost using a numerical performance model are detailed in [64].

C. Weather Forecast

Meteorological phenomena such as wind and temperature have an important influence on flight cost. The temperature affects engine performance, such as thrust, as higher temperatures tend to increase the fuel needed to generate the required thrust. The temperature influences speed as higher temperatures increase the speed of sound for a given altitude. With the same thrust, the wind influences the aircraft's speed, since a headwind reduces the aircraft's speed and tailwinds increase its speed. For these reasons, a realistic and accurate model was selected: the forecast data provided by Weather Canada.

FIGURE 1 Numerical performance model.

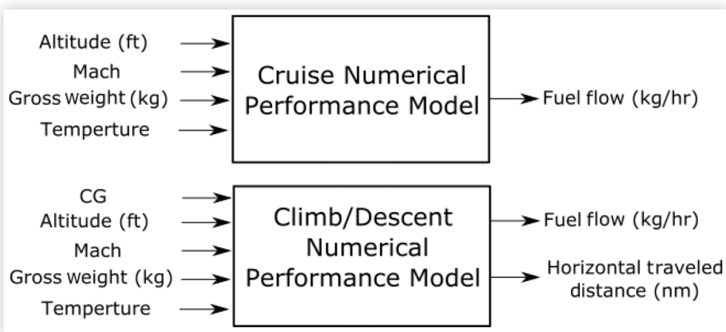

FIGURE 2 Weather interpolation sequence.

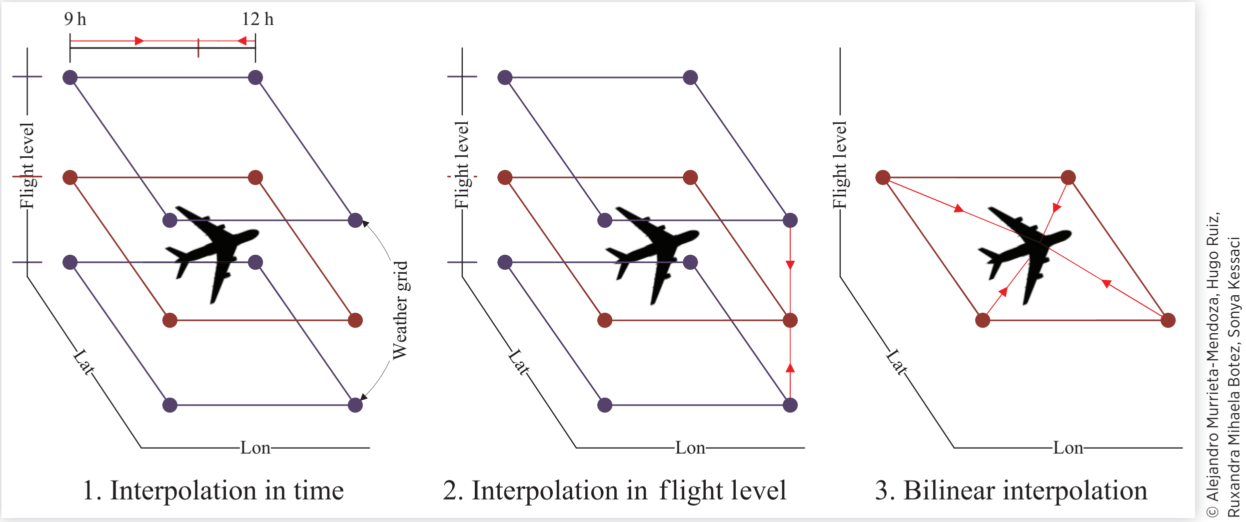

This forecast consists of a 0.6 km × 0.6 km grid at different pressures (altitudes). The grid is provided in 3-hour blocks beginning at 0h up to 144h. Information such as temperature, wind speed, and wind direction are available at each grid point. As the aircraft is rarely located at a grid's vortex, at the exact time and pressure altitude, interpolations in time and pressure altitude and, finally, bilinear interpolations in position are required to obtain the weather information at an exact point. The interpolation concept is explained in Figure 2.

The wind information is used to compute the Ground Speed (*GS*), in other words, the aircraft's speed relative to the ground, as indicated in Equation 2.

$$GS = TAS + WS * \cos(\varphi - WD) \qquad \text{Eq. (2)}$$

where True Air Speed (*TAS*) in knots (kts) is the aircraft's speed relative to the atmosphere, *WS* is the wind speed in kts, φ is the aircraft's heading, and *WD* is the wind direction [65]. This *GS* is used to compute the *Flight Time* needed in Equation 1.

II. Optimization Algorithm

A. Search Space

This algorithm takes advantage of the *free-flight* concept. Meaning that aircraft is not entirely subject to the ATC; thus it can travel almost anywhere in the airspace. It as well assumes that there is no potential conflict with other aircraft, and it can fly to any point within the airspace. This means that there is an infinite number of possibilities with which a reference trajectory may be created. Indeed a complex problem to solve. The search space is modeled under the form of n unidirectional graph. This is $G(V, E)$, where V stands for the nodes where the aircraft can fly and E stands for the links between the nodes. In the graph, every node is exclusively connected to its consecutive neighbors.

The search space can be divided into two different search spaces: the LNAV search space and the VNAV search space. The 3D search space is their combination. The search space for the LNAV and VNAV is explained next.

1. Search Space for the VNAV The vertical search space is located between the Top of Climb (ToC) and Top of Descent (ToD) and between the minimal and maximal altitudes. The ToC is the waypoint where the aircraft begins the cruise phase, and the ToD is the waypoint where the descent phase begins. However, this algorithm only focuses on the cruise-phase study and does not consider the descent phase. The maximal and minimal altitudes are defined between 26,000 ft and 41,000 ft, typical cruise altitudes for commercial flights. The search space for the VNAV is defined in Figure 3.

Nodes for the ground track are defined for the initial altitude. These nodes are replicated at every 2,000 ft to comply with ATM separation rules (eastbound flights travel at even altitudes and westbound flights travel at odd altitudes [66]). This node pattern is illustrated in Figure 4.

A change in altitude can take place only when the aircraft is at a node; therefore, the number of nodes selected to create the graph is very important because it has an impact on the algorithm's performance. If for a given flight, a high number of waypoints are placed, the search space will be more precise. However, more combinations would be possible; this would greatly increase the computation time. As suggested in [64], 34 nodes (waypoints) are selected and further distributed to create the reference trajectory, since this number of 34 waypoints provides a good compromise between short computation time and a good search space resolution that allows a reasonable amount of space exploration.

FIGURE 3 VNAV conceptual search space.

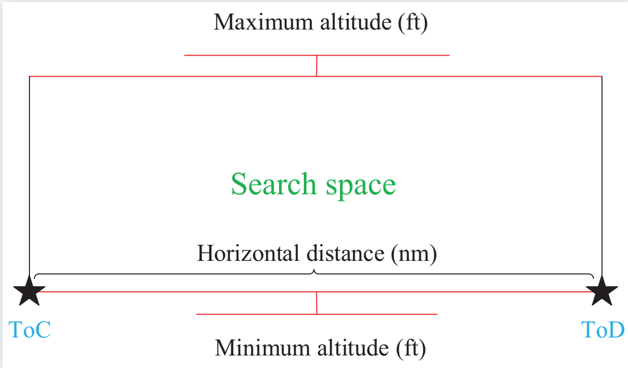

2. LNAV Search Space The search space for the LNAV consists of the direction changes an aircraft can execute during a flight. This search space is defined by two boundaries: the space between the ToC and the ToD, and the distance between the reference trajectory and the area to be covered. The trajectory of reference could be the great circle, called also the geodesic (the shortest distance between any two points on a sphere), between the departure and arrival airport, a precomputed trajectory, or a trajectory from the as-flown historical flight. The separation between two waypoints can have a value between 7.5 and 15 degrees. The search space for the LNAV is shown in Figure 5, where four different trajectories are parallel to the reference trajectory and α is the angle between two consecutive waypoints. Note that the aircraft can change headings to any consecutive node only when it is at a given node.

3. 3D Search Space The combination of the VNAV and LNAV provides a graph defining the search space for the whole flight, as shown in Figure 6.

FIGURE 4 Waypoints for the VNAV.

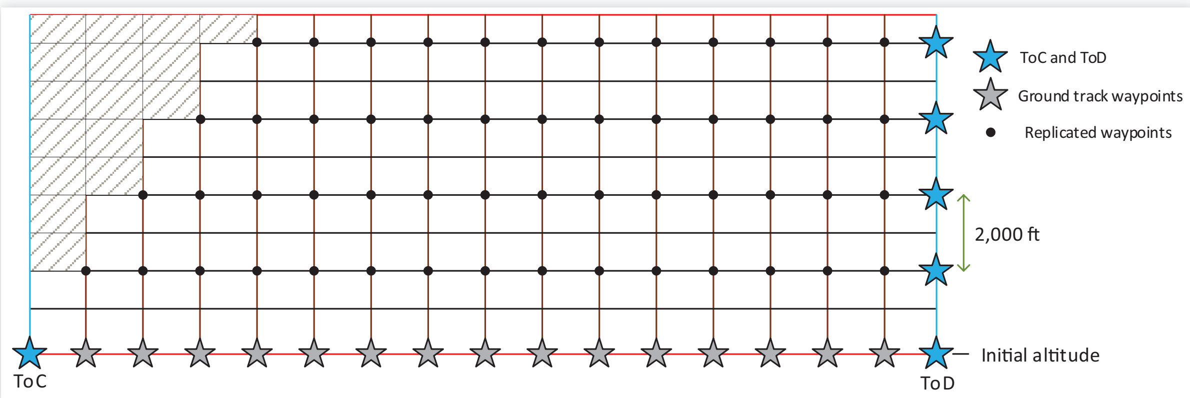

FIGURE 5 LNAV dimension.

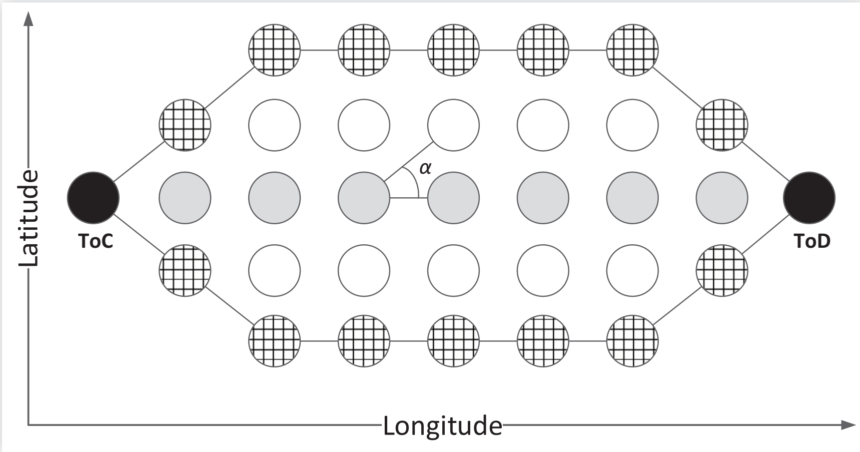

B. General PSO Algorithm

The PSO algorithm simulates animal behavior, such as that of a flock of birds and a school of fish. It differs from other algorithms inspired by bio-organisms, such as ant or bee colonies, because these animal societies do not have a leader; instead, they utilize the intelligence of the whole community. In the PSO algorithm, there is a temporary leader and all of the community is influenced by this leader.

The standard PSO algorithm operates through an iterative exploration of a given search space wherein three parameters can influence the current position of a given particle:

1. The position of the most economical particle among all the particles (called the *global optimal*)
2. The position of the most promising trajectory in a cluster of trajectories (called the *local optimal*)
3. The displacement of each particle

FIGURE 6 3D search space graph, a mix of the LNAV and VNAV.

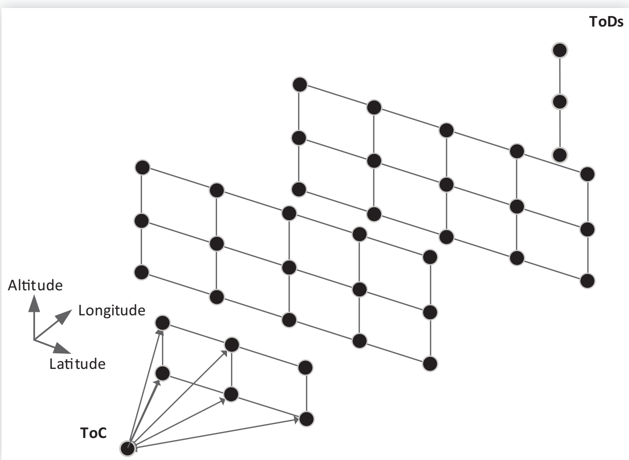

During the optimization process, particles move through the search space as influenced by global and local *leaders*. The search is thus directed to the current most economical conditions exploring the search space. This behavior is expressed in Equations 3 and 4.

$$D_i(k+1) = \omega R_\omega D_i(k) + c_1 R_1 \left(B_l - X_i(k)\right) + c_2 R_2 \left(B_g - X_i(k)\right) \quad \text{Eq. (3)}$$

$$X_i(k+1) = X_i(k) + D_i(k+1) \quad \text{Eq. (4)}$$

where i is the *current* particle and k is the current iteration. D is the computed displacement, X is the new particle's location, B_g is the global optimal particle position (most economical particle), and B_l is the best local particle position. Parameters c_1 and c_2 are positive constants, which influence the particle's displacements in reference to the global and local most-economical particles. The parameter ω refers to the particle's inertia, in other words, the particle's tendency to maintain the same direction. To create an arbitrary influence in convergence to the optimal solution, there are three random parameters with values between 0 and 1: R_ω, R_1, and R_2. The role of these R parameters is to determine the influence of ω, B_l, and B_g, respectively, on the particle's movement.

By computing Equations 3 and 4 for a given number of iterations, the search space can be explored and the optimal solution found. However, considerations should be taken into account to adapt this algorithm to the reference trajectory optimization problem, as discussed next.

C. Consideration for the PSO Algorithm for the Reference Trajectory Optimization in 4D

For the purposes of the developed algorithm, a complete trajectory defines a particle. This complete trajectory is defined as a set of waypoints linking the ToC to the ToD. For example, a vector WPT contains n waypoints for a given trajectory, as shown in Equation 5.

$$WPT = \left[wpt_i^1, wpt_i^2, \ldots, wpt_i^n \right] \quad \text{Eq. (5)}$$

where WPT contains the position, altitude, and speed for each waypoint defining the trajectory i. When Equations 3 and 4 are executed, the waypoints' information is being modified, as influenced by the local and global optimal solutions exploring the search space. However, displacements D could lead to positions X that are outside of the search space. For this reason, after a displacement at each iteration, the algorithm verifies if the trajectory is within the search space.

1. VNAV Verification The first verification consists of ensuring that the resulting new position X contains altitudes that are exactly at 1,000 ft multiples. Altitudes that do not comply with this condition are identified from vector X and are rounded to their closest 1,000 ft multiple values (e.g., 34,321 ft is rounded to 34,000 ft).

The other set of verifications are related to disparities in the trajectory's shape, consecutive altitude changes, and being outside of the search space. Some typical situations that require correction are shown in Figure 7 and explained in the next paragraph. Then the corrected trajectory will have the shape shown in Figure 8.

For the first disparity (number 1 in Figure 7), the trajectory tries to descend to altitudes outside the boundary limits: the algorithm will fix the waypoints at the minimum altitude available for the flight to stay within the altitudes limits.

The second disparity is the aircraft descending to out-of-bounds altitudes.

FIGURE 7 Typical VNAV discrepancies.

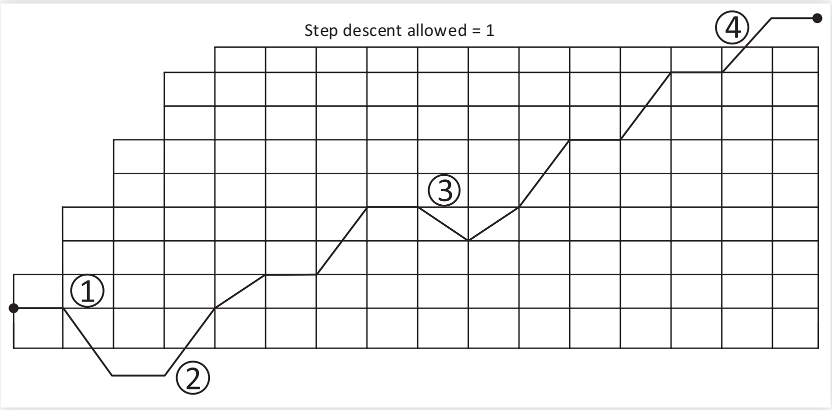

FIGURE 8 Vertical reference trajectories after corrections.

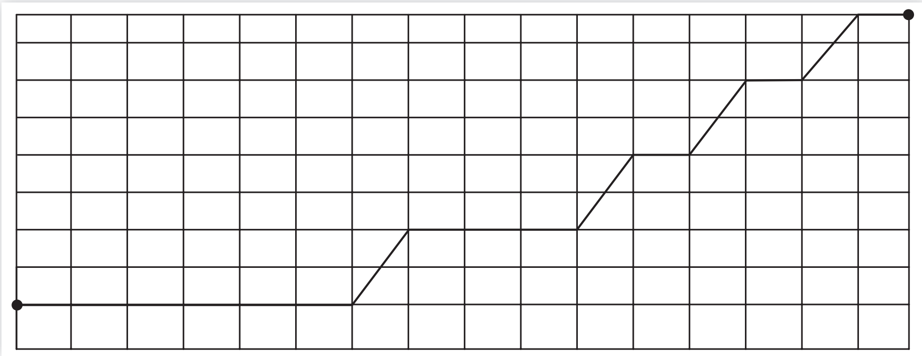

The third disparity occurs at two consecutive changes of altitude. Under normal circumstances, the aircraft stays at a constant altitude for a certain time after a change of altitude.

The aircraft would make a step descent, followed by a climb at the next few waypoints. Moreover, the proposed step climb is only 1,000 ft. This disparity may be absurd and it would increase the ATC workload to obtain clearance for this procedure. The algorithm will also cancel this descent so the aircraft maintains the same altitude as before. The algorithm will cancel this change of altitude, thus the current altitude is kept.

Finally, at the fourth disparity, the aircraft would attempt to reach an altitude higher than the maximum altitude: the algorithm would limit the altitude to that at the waypoint.

The corrected trajectory takes the shape indicated in Figure 8.

2. LNAV Verification For the LNAV, the algorithm selects only three consecutive waypoints: the one just in front and the ones separated by plus/minus the deviation angle α. This selection is shown in Figure 9, where waypoints 1 and 5 should not be selected.

Similar to the VNAV, the lateral waypoint selection may lead to incorrect waypoints being selected, and thus corrections are needed. Typical discrepancies for the LNAV are shown in Figure 10.

In the LNAV selection, the first discrepancy consists of a waypoint selection that is not one of the three closest consecutive waypoints. The algorithm corrects by selecting the closest valid waypoint.

The second type of discrepancy, shown by numbers 2 and 3, is the selection of a nonexistent waypoint located outside the boundaries. The algorithm corrects this discrepancy by selecting the boundary waypoint. After fixing all of these discrepancies, the valid trajectory takes the shape shown in Figure 11.

FIGURE 9 Consecutive waypoints selection.

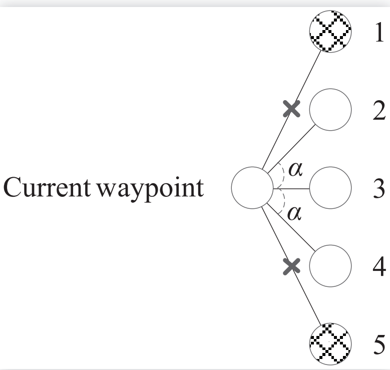

3. Managing the Difference between the Actual Flight Time and the RTA The optimization algorithm first computes an economical 3D trajectory (this trajectory may not fulfill the RTA constraint), then it adjusts the Mach number over that 3D trajectory to fulfill the RTA constraint.

However, when computing the optimal trajectory in 3D, the solution may deliver a trajectory that would not fulfill the RTA constraint. An artificial value is therefore added to the real cost; this measure ensures that trajectories that are not likely to fulfill the RTA constraint will be rejected. The flight cost is then computed with Equation 6. Note that this cost will not be reflected in the final trajectory cost; instead, this cost is only used to reject trajectories. The real flight cost is still computed using Equation 1:

$$Artificial\ Flight\ Cost = Fuel\ Burn + Cost\ Index * Flight\ Time + Cost_{RTA} \quad \text{Eq. (6)}$$

FIGURE 10 Typical LNAV discrepancies.

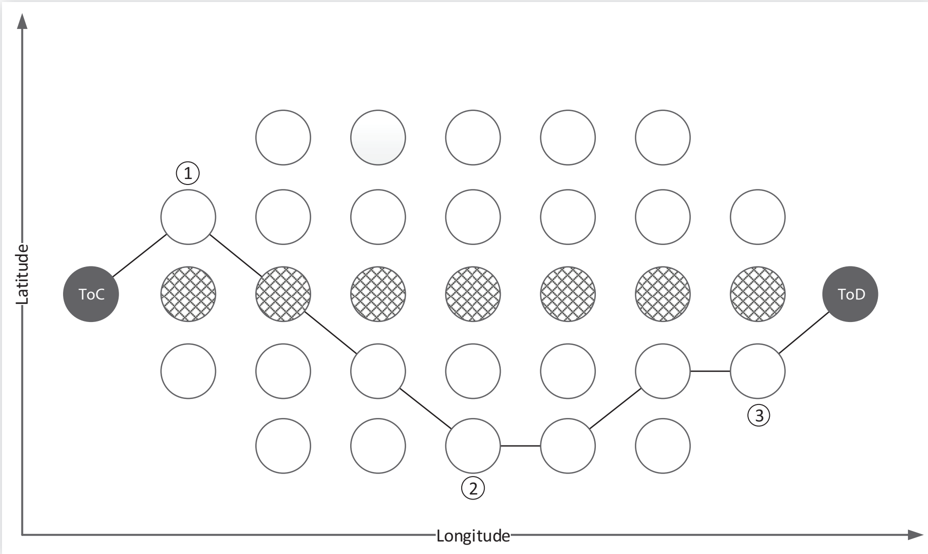

where $Cost_{RTA}$ corresponds to the artificial cost of not arriving on time to the trajectory. This parameter is computed differently, depending on the circumstances. Three main cases with different circumstances are defined next:

a. When the aircraft fulfills the RTA constraint $Cost_{RTA}$ equals 0.
b. When the aircraft arrives slightly late/early to the destination, $Cost_{RTA}$ is computed using Equation 7

$$Cost_{RTA} = \Delta Time * CTC \qquad \text{Eq. (7)}$$

where $\Delta Time$ is the difference between the RTA and the actual trajectory flight time (in hours), and CTC is the Current Trajectory Cost. This small cost will cause the algorithm to favor trajectories with the flight time closer to the RTA when two or more trajectories provide similar flight costs.

FIGURE 11 LNAV after corrections.

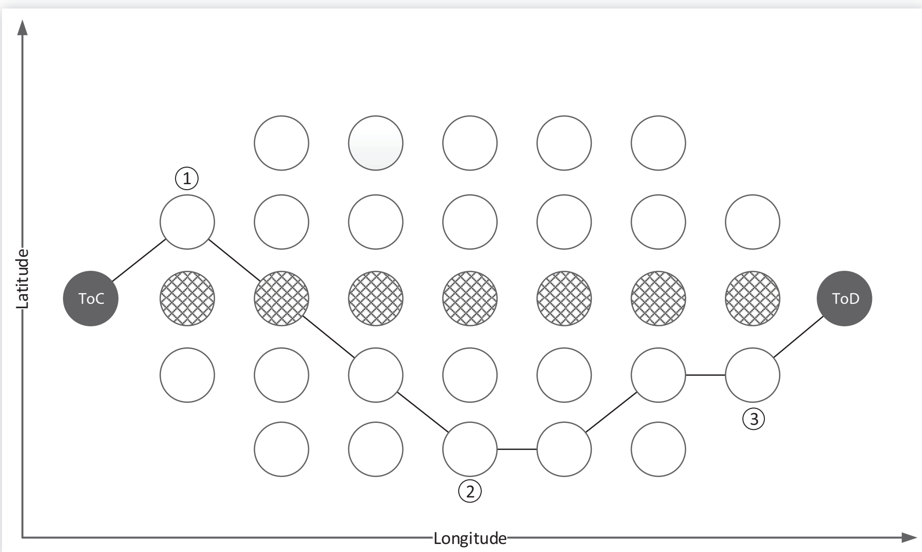

FIGURE 12 4D reference trajectory algorithm flowchart.

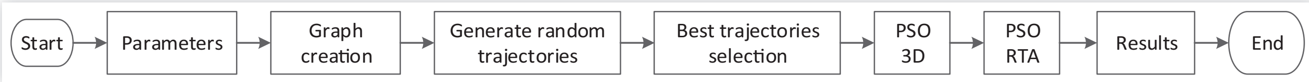

FIGURE 13 PSO implementation in 4D reference trajectory.

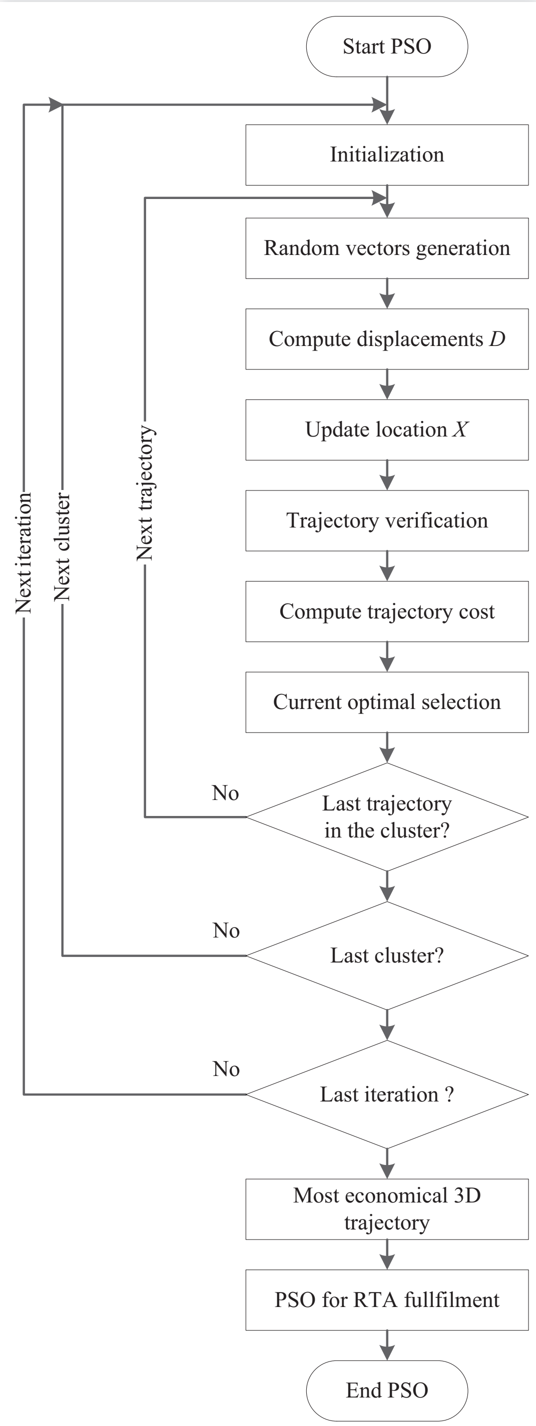

c. When the aircraft is significantly late/early, $Cost_{RTA}$ is computed using Equation 8

$$Cost_{RTA} = 1.1 * CTC + \Delta\, Time * CTC \qquad \text{Eq. (8)}$$

Note that, as in Equation 8, when the aircraft arrives significantly late to the destination, 10% of the *CTC* is added to the time difference. This high cost will cause the algorithm to reject that type of trajectory.

D. The Developed Optimization Algorithm

First, the proposed algorithm computes the 3D optimization trajectory without necessarily fulfilling the RTA constraint. Next, the algorithm will adjust the combination of Mach numbers defined for the 3D trajectory to fulfill the RTA constraint.

The optimization algorithm operates by following the blocks indicated in Figure 12.

In Figure 12, information such as the number of waypoints, the total graph size (search space), the reference waypoints definition, the number of clusters, trajectories per cluster, initial and final coordinates, and the RTA constraint are defined in the *Parameters* block.

The *Graph Creation* block defines the waypoints and the connections between the waypoints that define the search space. The block *Generate random trajectories* generates the first set of trajectories and arbitrarily gathers them in different clusters. The *Best trajectories selection* block evaluates the flight cost and the flight time for each trajectory, identifies the most economical trajectory for each cluster, and identifies the most economical trajectory from each cluster. The *PSO* block, explained next, finds the most economical trajectory that fulfills the RTA constraint. Finally, the *Results* block displays the flight cost and the proposed trajectory.

The PSO module is somewhat complex; its function is defined in the flowchart presented in Figure 13, each block of which is explained next.

Initialization

Parameters, such as the different trajectories coordinates and altitudes, are recovered.

Random Vectors

Vectors R_w, R_1, and R_2 are generated using a stochastic function. These vectors are generated for each displacement.

Compute the Particle Displacements

Displacements $D(k + 1)$ are computed using Equation 3. The displacement is computed for each dimension: altitude, speed, and heading.

Position Update

The particle's position $X(k + 1)$ is updated using Equation 4. In other words, the altitude, speed, and aircraft position are updated to reflect the previously computed displacements D.

Trajectory Verification

The trajectory is verified and, if required, modified to avoid its discrepancy, as explained in Section II.c.1 and Section II.c.2.

Trajectory Cost Computation

The cost of the new trajectory is computed using Equation 6; this means that the artificial cost is taken into account to deliver a 3D reference trajectory close to the required RTA, as discussed in Section II.c.3.

Current Optimal Selection

The new local best and new global best are identified. If the current local best within a given cluster is more expensive than any of the newly generated trajectories, then the most economical trajectory becomes the new local best. If any of the local best trajectories are more economical than the current global best, then the most-economical trajectory becomes the global best. If the total number of iterations is reached, the algorithm ends; otherwise, the algorithm returns to the *Initialization* block.

Trajectory Option Set (TOS)

Because the algorithm is using each cluster's local optimal to influence the global optimal, the local optimal, which are suboptimal, are still good solutions. These local solutions are extracted from the algorithm and are presented as the TOS, which can be used if the optimal trajectory can no longer be followed due to traffic or a sudden change of ATM constraints.

PSO for RTA Fulfillment

In this last block of Figure 13, the algorithm modifies the Mach numbers in the precomputed 3D trajectory. This block is where the PSO is executed to determine the Mach number that will fulfill the RTA constraint. In other words, the algorithm computes the Mach number combination that reduces the flight cost while fulfilling the RTA constraint. This last block takes the form shown in Figure 14. The displacements and the particle's position only change in terms of Mach number (speed). A unique trajectory is being modified by utilizing only one parameter (Mach number).

The output of this block is an economical 4D reference trajectory that complies with the given RTA constraint.

FIGURE 14 Algorithm flowchart for the selection of Mach numbers that fulfill the RTA constraint.

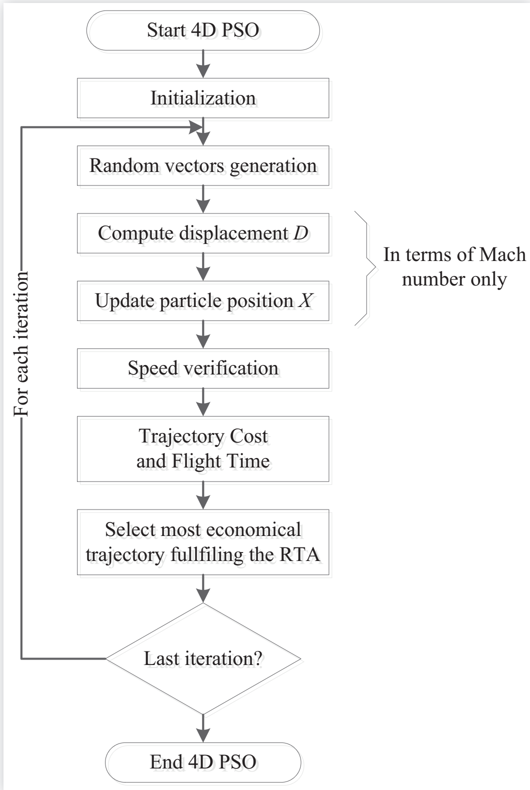

III. Results

Three different types of tests were performed to validate the PSO algorithm's ability to propose economic 4D flight reference trajectories for a commercial aircraft. The aircraft selected for these flight tests is a two-engine long-haul European aircraft with a ceiling altitude of 41,000 ft, Mach number range from 0.6 to 0.82, flight range of around 5,000 nm, a maximal takeoff weight of around 160 tons, and a carrying capacity of approximately 220 passengers.

The three different types of tests were designed to evaluate the algorithm's saving capacity utilizing three different types of trajectories, the lateral, the vertical, and the 3D. Firstly, the VNAV and the LNAV contributions to the 3D flight optimization were evaluated. Secondly, the 3D trajectories costs were compared to that of the 4D optimized trajectory to evaluate the difference, if any, between 3D and 4D optimized trajectories. Thirdly, the flight calculated by the algorithm was evaluated against an *as-flown flight* obtained from open-source data provided by *flightaware*®.

However, as the aircraft's gross weight is not provided, a gross weight of 125 tons was used for all tests, as it is a *normal* gross weight at the ToC for this type of commercial aircraft. A Cost Index of 50 was used for all flights. This Cost Index was used as it is the Cost Index used by a European airliner using this same aircraft. The weather was taken into account for all flights. The PSO parameters for all of these tests are shown in Table 1.

TABLE 1 PSO parameters.

Parameter	Value
Number of clusters	5
Trajectories per cluster	25
Total iterations	100
Possible step climbs	Unlimited
Possible descents	1

A. Vertical, Lateral, and 3D Optimization

The set of tests in this section serves two different objectives:

1. To validate that the algorithm can optimize in any dimension (lateral, vertical, and 3D).
2. To observe that the optimized trajectories values are within the range of their normal optimized values.

For testing purposes, the fuel consumption was calculated for four different flights: Montreal (YUL)-Paris (CDG) on a distance of about 2,970 nm, Toronto (YYZ)-London (LDH) with a distance of 3,080 nm, Montreal (YUL)-Vienna (VNN) on a distance of 3,300 nm, and Vancouver (YVR)-Gran Canaria (LPA) on a distance of 4,770 nm. The fuel consumption for a Cost Index of 50 was evaluated (Figure 15) for the LNAV, the VNAV, and the simultaneous combination of both the LNAV and the VNAV, or the 3D trajectory. The LNAV allows a change of heading at a constant altitude, the VNAV allows only a change of altitude following the geodesic ground-fixed trajectory, and the 3D trajectory allows both: a change of heading and a change of altitude. The reference trajectory was taken at a fixed altitude following the geodesic trajectory at a fixed altitude of 32,000 ft.

As expected, different types of trajectories provided different optimized fuel consumption values. The LNAV provided very little optimization opportunities. This result was expected as an aircraft depends mostly on winds to reduce fuel burn. The VNAV optimization contributes much more to the fuel consumption optimization because changing altitudes brought an aircraft to those conditions where temperature (and probably the wind directions) contributes most to the aircraft operation. Finally, the 3D optimization provided the highest savings; the total 3D optimized trajectories savings is roughly the sum of the lateral and the vertical optimized trajectory savings.

These results serve to validate that the solutions provided by the PSO reference trajectory algorithm are logical and in agreement with previous work discussed in the literature [30, 41, 54].

B. 4D Optimization for Simple Trajectories

The PSO algorithm provides an economical 3D reference trajectory from which the Mach numbers along the trajectory are adjusted to reach a given RTA constraint, creating

FIGURE 15 Fuel consumption optimization for four different flights with three different types of trajectories.

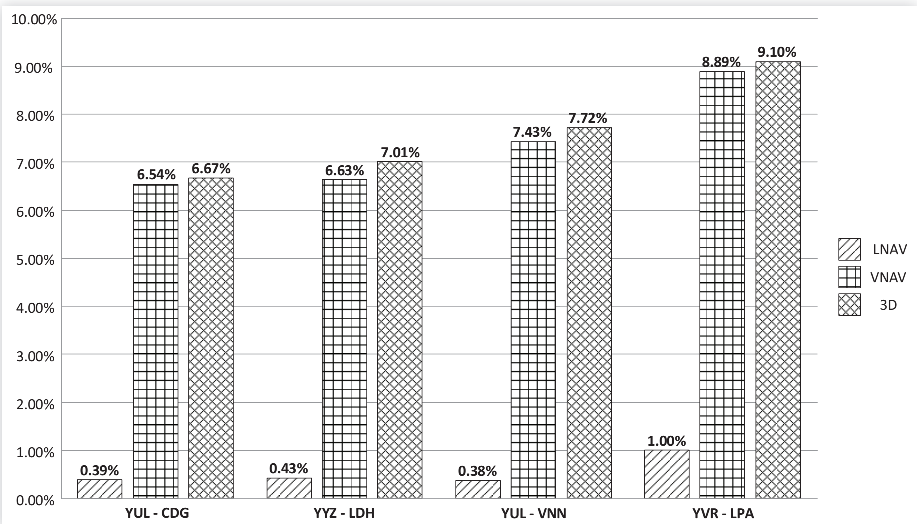

FIGURE 16 Fuel consumption comparison between the 3D and 4D optimized trajectories by varying the Mach number.

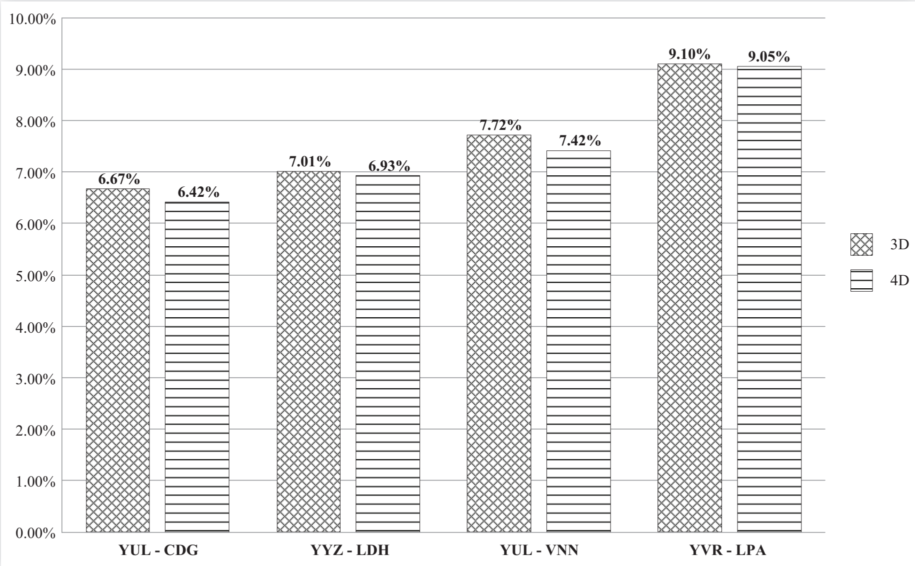

a 4D trajectory. The 3D flights are the same as those utilized in the previous subsection and shown in Figure 15. The only difference is that the set of Mach numbers was modified to comply with the RTA constraint (4D trajectory). The fuel consumption savings percentages of the 3D and 4D trajectories are shown in Figure 16.

As shown in Figure 16, the 4D trajectory optimization slightly reduced the fuel savings achieved by 3D optimization. This reduction was due to the less-efficient speeds selected to fulfill the RTA constraint in 4D optimization, while the 3D reference trajectory optimization algorithm always selected the most economical set of Mach numbers. However, these results confirm that only a small *loss of optimization* occurred because of the aim to achieve the required RTA.

Table 2 shows the Estimated Time of Arrival (ETA) for the delivered 3D and 4D trajectories and their comparison to the RTA.

The flight time results in Table 2 show that the ETA for the 4D reference trajectory (column 7) was always within the imposed tolerance limits (column 3). The ETA for the 3D reference trajectory was consistently further from the required ETA; however, it was observed that the maximum difference was around 30 seconds because the algorithm proposed 3D trajectories that were not far from the RTA due to the artificial flight cost explained in Section III.C.3. This artificial flight cost allowed the algorithm to select near-RTA fulfillment trajectories.

TABLE 2 RTA fulfillment for the 4D reference trajectory.

Flight	RTA	Tolerance (s)	ETA 3D	Difference 3D ETA (s)	ETA 4D	Difference 4D ETA (s)
YUL-CDG	16h50m42s	30	16h51m52s	69	16h50m18s	24
YYZ-LDH	17h03m32s	30	17h04m20s	48	17h03m06s	25
YUL-VNN	17h42m24s	30	17h41m20s	63	17h41m56s	27
YVR-LPA	20h40m56s	30	20h42m06s	69	20h41m06s	9

TABLE 3 4D trajectory optimization RTA fulfillment.

Flight	Real flight fuel burn (kg)	Optimized flight (kg)	Difference (kg)	RTA	4D ETA	Difference (s)
YYC-CUN	29,123	28,719	404 (1.39%)	22h07m46s	22h07m56s	10
YEG-PUJ	42,170	41,594	576 (1.37%)	19h44m48s	19h44m33s	15
YYC-VRA	33,458	32,849	609 (1.82%)	15h40m54s	15h40m31s	23
YYZ-DUB	25,296	24,422	873 (3.45%)	10h46m40s	10h46m12s	-28
BRU-YUL	24,382	23,810	572 (2.34%)	19h50m24s.	19h51m00s	24
GLA-YYZ	23,870	23,296	574 (2.4%)	19h45m00s	19h45m12s	12
YYZ-CDG	25,493	24,788	705 (2.7%)	20h09m00s	20h08m57s	3

C. Real Flight Reference Trajectory Optimization

This set of tests was designed to evaluate the PSO flight optimization against *as-flown* trajectories obtained from flightaware®. These trajectories were flown with the same aircraft as the one used earlier in this article (detailed at the beginning of this section). The flight information for three long-haul flights: Calgary (YYC) to Cancun (CUN), Edmonton (YEG) to Punta Cana (PUJ), and YYC to Varadero (VRA), is shown in Table 3. The selected RTA that the algorithm had to fulfill was the reported time of arrival for the selected as flown flights. This RTA had a 30-second tolerance.

As it can be observed in Table 3, the algorithm was able to reduce the fuel burn and meet the RTA constraint within the imposed 30-second limit. This performance was possible because the algorithm could give better altitudes and take advantage of winds. The LNAV and the VNAV proposed by the 4D reference trajectory algorithm were compared to the as-flown trajectory for one flight in Figures 17 and 18, respectively. The optimal trajectory is represented in orange, and the *as-flown* trajectory is shown in blue.

FIGURE 17 LNAV and the search space limit for the Calgary-to-Punta Cana flight.

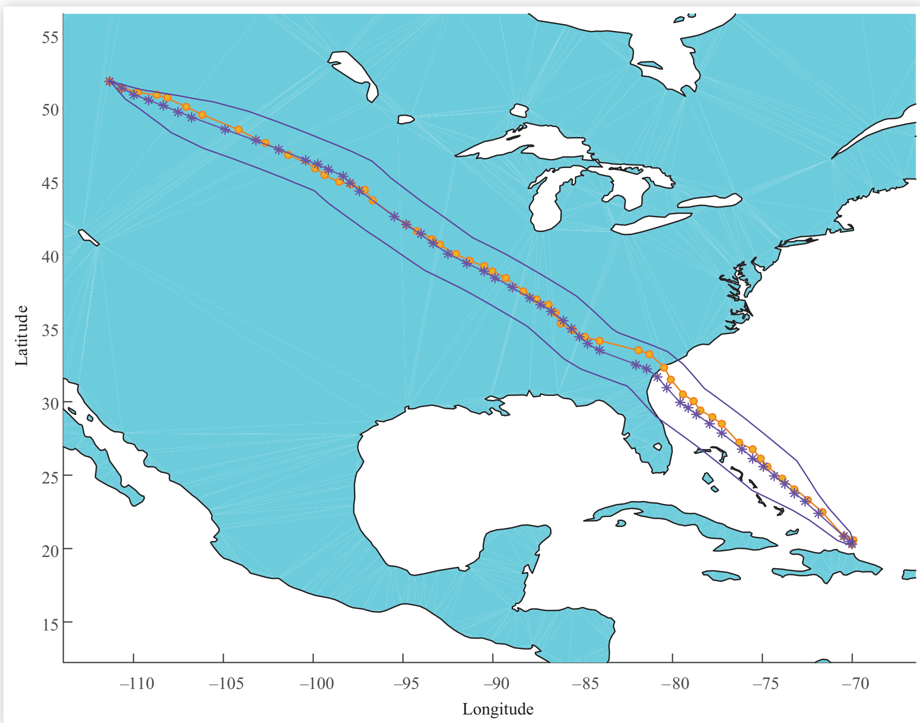

FIGURE 18 VNAV and the search space limits for the Calgary-to-Punta Cana flight.

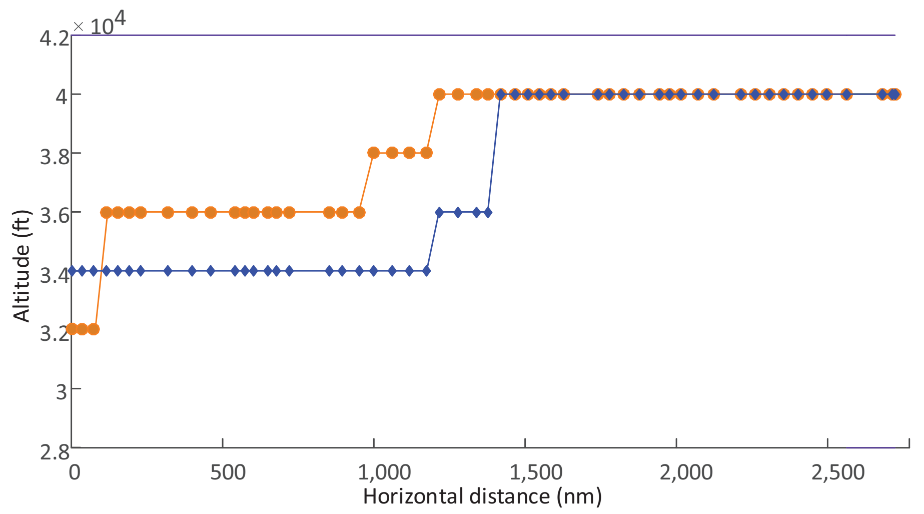

As shown in Figure 17, the optimal lateral trajectory diverges slightly from the reference trajectory, in this case, due to favorable winds. The VNAV is quite similar to the real flight trajectory as shown in Figure 18, with the main difference that the developed algorithm proposed beginning the cruise phase at 32,000 ft instead of 34,000 ft. The vertical trajectory delivered by the PSO algorithm proposed three 2,000 ft step climbs, and the *as-flown* algorithm executed only two step climbs: one 2,000 ft step climb and one 4,000 ft step climb. Both flights ended at the same altitude (40,000 ft). These small differences provided the fuel savings reported in the last column of Table 3.

D. Flight Optimization and TOS

This set of tests aims to evaluate the trajectories alternatives proposed by the PSO algorithm. As explained in Section II.B, the PSO algorithm gathers the solutions in different groups, each group has a leader (local optimal). By extracting these local optimal, a set of alternative trajectories could be provided. Figure 19 shows the lateral reference alternative trajectories to be followed (the local optimal), and Figure 20 shows the vertical reference alternative trajectories to be followed for the intercontinental flight between DUB and YYZ in Table 3. Figure 19 shows how the local trajectories tend to follow waypoints in the north of the search space. It can also be seen that the optimal trajectory, as well as the set of alternative trajectories, are close to each other. Figure 20 shows that most of the trajectories (including the as-flown trajectory) end at 38,000 ft., except for one that ends at 36,000 ft. All trajectories execute step climbs. It should be noted that Local Trajectory 3 is also the global optimal.

Figure 21 shows the fuel burn between all trajectories.

The last bar is the optimal trajectory and it is taken as a reference. It can be seen that the worst option trajectory is only 0.38% more expensive than the optimal trajectory. However, it was found that not all alternatives that fulfill the RTA show wind differences as high as 65 seconds from the RTA goal.

IV. Conclusion

A 4D reference trajectory optimization algorithm was developed using a numerical performance model and taking into account weather parameters such as winds and temperatures. Linear interpolations were required to obtain the desired values from the

FIGURE 19 TOS for the flight DUB-YYZ in the lateral dimension.

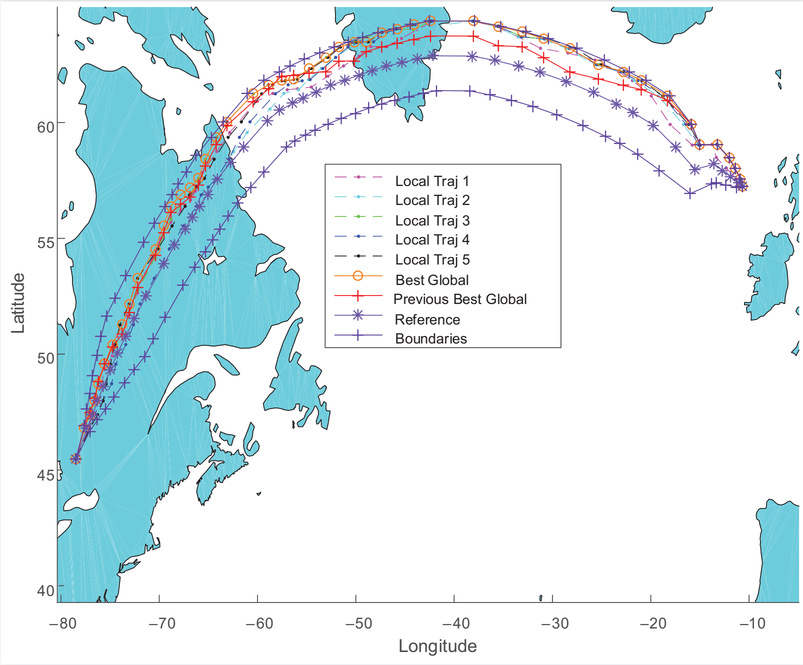

FIGURE 20 TOS for the flight DUB-YYZ in the vertical dimension.

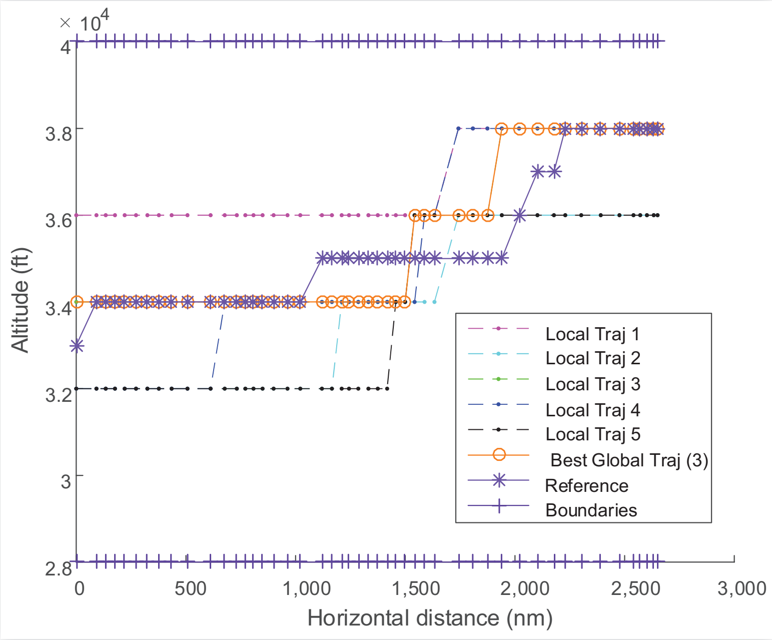

FIGURE 21 TOS cost difference.

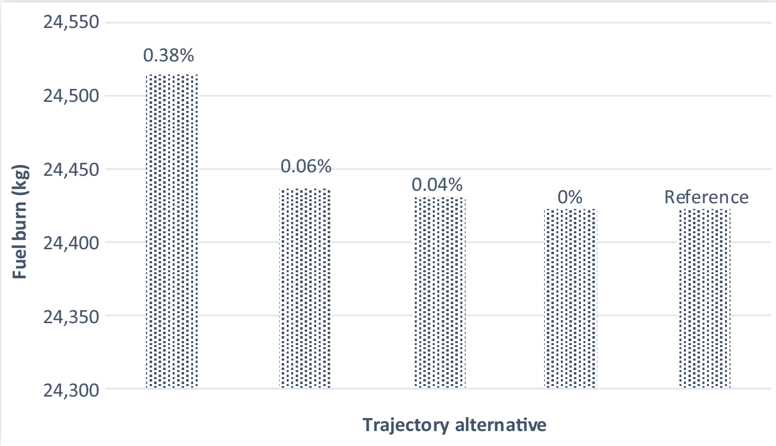

numerical performance model. Linear and bilinear interpolations were also executed to obtain the weather parameters at the aircraft's position.

The search space was modeled under the form of a graph to allow a finite number of solutions. The PSO algorithm was used to find the most-economical combinations of waypoints while fulfilling the RTA constraint. A trajectory verification was performed to obtain conventional trajectories such as fixed altitude segments and to keep the trajectory within the search space.

The first set of results compared the PSO savings' capabilities to those of simple trajectories. The results for the LNAV, VNAV, and 3D reference trajectory showed that the order of optimization for each of the beforehand dimensions agreed with the results shown in the literature. The first conclusion is that the algorithm provides logical and good results.

The second set of results showed that the as-delivered 3D trajectories were able to fulfill the RTA constraint (4D) after a Mach number modification. These results led to a second conclusion that the artificial cost added to reject 3D trajectories far from the imposed constraint is able to efficiently favor valid trajectories, as well as a third conclusion that the algorithm was able to modify the Mach number to fulfill the RTA constraint within the imposed tolerance.

The PSO reference trajectory results were compared with the results of as-flown flights obtained from *flightaware*®. For the three analyzed flights, the algorithm was able to provide slight changes to the *as-flown* trajectory and to deliver flights that reduced fuel consumption while arriving very close to the same time as the real flights. This result supports the last conclusion that the algorithm is able to deliver trajectories that are more economical than as-flown trajectories under the provided conditions.

The last set of results showed that the algorithm, by its nature of working with different particle leaders that are influencing the optimization, provides a TOS. In this set, suboptimal trajectories are obtained, which are still close to the optimal ones.

For future work, it would be desirable to evaluate this algorithm by taking into account the descent phase, as well as to evaluate this algorithm in the presence of traffic and obstacles. Another improvement opportunity is to improve the RTA for the trajectories options set. Finally, it will be desirable that the algorithm should be able to solve as well potential conflicts with another aircraft and take operational indices such as safety and workload to evaluate its use in a real ATM environment.

References

1. Crutzen, P.J., "The Influence of Nitrogen Oxides on the Atmospheric Ozone Content," *Q.J.R. Meteorol. Soc.* 96(408):320-325, 1970, https://doi.org/10.1002/qj.49709640815.
2. Robinson, E., "Hydrocarbons in the Atmosphere," *Pure and Applied Geophysics* 116(2-3):372-384, 1978, https://doi.org/10.1007/bf01636892.
3. ATAG, *Aviation Benefits Beyond Borders* (Geneva, Switzerland: Air Transport Action Group, 2014).
4. ICAO, *Aviation's Contribution to Climate Change* (Montreal: International Civil Aviation Organization, 2010), 260.
5. Williams, P.D., "Transatlantic Flight Times and Climate Change," *Environmental Research Letters* 11(2):024008, 2016, http://doi.org/10.1088/1748-9326/11/2/024008.
6. Randt, P.N., Jessberger, C., and Ploetner, K.O., "Estimating the Fuel Saving Potential of Commercial Aircraft in Future Fleet-Development Scenarios," in *15th AIAA Aviation Technology, Integration, and Operations Conference*, American Institute of Aeronautics and Astronautics, Dallas, TX, 2015.
7. McConnachie, D., Wollersheim, C., and Hansman, R.J., "The Impact of Fuel Price on Airline Fuel Efficiency and Operations," in *2013 Aviation Technology, Integration, and Operations Conference*, American Institute of Aeronautics and Astronautics, Los Angeles, California, USA, 2013.
8. Kwok-On, T., Daniel, B., and Anthony, W., "Development of Continuous Descent Arrival (CDA) Procedures for Dual-Runway Operations at Houston Intercontinental," in *6th AIAA Aviation Technology, Integration and Operations Conference (ATIO)*, American Institute of Aeronautics and Astronautics, Wichita, Kansas, USA, 2006.
9. Ribeiro, V.F., Pamplona, D.A., Fregnani, J.A.T.G., Oliveira, Í.R.d. et al., "Modeling the Swarm Optimization to Build Effective Continuous Descent Arrival Sequences," in *2016 IEEE 19th International Conference on Intelligent Transportation Systems (ITSC)*, Rio de Janeiro, Brazil, 2016, 760-765.
10. Seenivasan, D.B., Olivares, A., and Staffetti, E., "Optimal 4D Trajectory Planning for Multiple Aircraft in Continuous Descent Operations," in *8th European Conference for Aeronautics and Aerospace Sciences (EUCASS)*, Madrid, 2019.
11. Murrieta-Mendoza, A., Botez, R.M., and Ford, S., "New Method to Compute the Missed Approach Fuel Consumption and Its Emissions," *The Aeronautical Journal* 120(1228):18, 2016, http://doi.org/10.1017/aer.2016.37.
12. Dancila, R., Botez, R.M., and Ford, S., "Fuel Burn and Emissions Evaluation for a Missed Approach Procedure Performed by a B737-400," *The Aeronautical Journal* 118(1209):20, 2014.
13. Jensen, L., Hansman, J.R., Venuti, J., and Reynolds, T., "Commercial Airline Altitude Optimization Strategies for Reduced Cruise Fuel Consumption," in *14th AIAA Aviation Technology, Integration, and Operations Conference*, American Institute of Aeronautics and Astronautics, Atlanta, Georgia, 2014.
14. Jensen, L., Hansman, J.R., Venuti, J.C., and Reynolds, T., "Commercial Airline Speed Optimization Strategies for Reduced Cruise Fuel Consumption," in *2013 Aviation Technology, Integration, and Operations Conference*, American Institute of Aeronautics and Astronautics, Los Angeles, 2013.
15. Turgut, E.T., Cavcar, M., Usanmaz, O., Canarslanlar, A.O. et al., "Fuel Flow Analysis for the Cruise Phase of Commercial Aircraft on Domestic Routes," *Aerospace Science and Technology* 37(0):1-9, 2014, http://doi.org/10.1016/j.ast.2014.04.012.
16. Field, A., *International Air Traffic Control : Management of the World's Airspace* (Oxford; New York: Pergamon Press, 1985).
17. Liden, S., "Practical Considerations in Optimal Flight Management Computations," *Journal of Guidance, Control, and Dynamics* 9(4):427-432, 1986, https://doi.org/10.2514/3.20128.

18. Liden, S., "Optimum Cruise Profiles in the Presence of Winds," in *Digital Avionics Systems Conference, 1992. Proceedings., IEEE/AIAA 11th*, Seattle, WA, 1992, 254-261.

19. Pargett, D.M. and Ardema, M.D., "Flight Path Optimization at Constant Altitude," *Journal of Guidance, Control, and Dynamics* 30(4):1197-1201, 2007, https://doi.org/10.2514/1.28954.

20. Rosenow, J., Strunck, D., and Fricke, H., "Trajectory Optimization in Daily Operations," *CEAS Aeronautical Journal* 11(2):333-343, 2019, https://doi.org/10.1007/s13272-019-00429-7.

21. Dhief, I., Delahaye, D., Dougui, N.H., and Rodionova, O., "Comparison between Two Wind-Optimal Strategic Flight Plannings for North Atlantic Traffic," *Journal of Air Transportation* 27(1):26-38, 2019, https://doi.org/10.2514/1.D0110.

22. Dancila, B., Botez, R.M., and Labour, D., "Fuel Burn Prediction Algorithm for Cruise, Constant Speed and Level Flight Segments," *The Aeronautical Journal* 117(1191):491-504, 2013.

23. Valenzuela, A. and Rivas, D., "Optimization of Aircraft Cruise Procedures Using Discrete Trajectory Patterns," *Journal of Aircraft* 51(5):1632-1640, 2014, http://doi.org/10.2514/1.C032041.

24. Félix-Patrón, R.S., Botez, R.M., and Labour, D., "New Altitude Optimisation Algorithm for the Flight Management System CMA-9000 Improvement on the A310 and L-1011 Aircraft," *The Aeronautical Journal* 117(1194):787-805, 2013.

25. Murrieta-Mendoza, A., Beuze, B., Ternisien, L., and Botez, R., "Branch & Bound-Based Algorithm for Aircraft VNAV Profile Reference Trajectory Optimization," in *15th AIAA Aviation Technology, Integration, and Operations Conference, Aviation Forum*, AIAA, Dallas, TX, 2015.

26. Murrieta-Mendoza, A. and Botez, R.M., "Vertical Navigation Trajectory Optimization Algorithm for a Commercial Aircraft," in *AIAA/3AF Aircraft Noise and Emissions Reduction Symposium*, 2014, http://doi.org/10.2514/6.2014-3019.

27. Murrieta-Mendoza, A. and Botez, R.M., "Aircraft Vertical Route Optimization Deterministic Algorithm for a Flight Management System," SAE Technical Paper 2015-01-2541, 2015, https://doi.org/10.4271/2015-01-2541.

28. Murrieta-Mendoza, A., Mugnier, P., and Botez, R.M., "Vertical Reference Trajectory Optimization and Simulation for a Commercial Aircraft," in *11th International Conference on Modeling, Optimization and Simulation - MOSIM'16*, Montreal, QC, Canada, 2016.

29. Sidibe, S. and Botez, R.M., "Trajectory Optimization of FMS-CMA 9000 by Dynamic Programming," in *ASI AÉRO 2013 Conference, 60th Aeronautics Conference and AGM*, Toronto, Canada, 2013.

30. Murrieta-Mendoza, A., Félix-Patrón, R.S., and Botez, R.M., "Flight Altitude Optimization Using Genetic Algorithms Considering Climb and Descent Costs in Cruise with Flight Plan Information," SAE Technical Paper 2015-01-2542, 2015, https://doi.org/10.4271/2015-01-2542.

31. US Department of Transportation, FAA, "The Future of the NAS," Washington, DC, 2016.

32. Campbell, S.E., Bragg, M.B., and Neogi, N.A., "Fuel-Optimal Trajectory Generation for Persistent Contrail Mitigation," *Journal of Guidance, Control, and Dynamics* 36(6):1741-1750, 2013, https://doi.org/10.2514/1.55969.

33. Soler-Arnedo, M., Hansen, M., and Zou, B., "Contrail Sensitive 4D Trajectory Planning with Flight Level Allocation Using Multiphase Mixed-Integer Optimal Control," *AIAA Guidance, Navigation, and Control (GNC) Conference. American Institute of Aeronautics and Astronautics*, 2013.

34. Sridhar, B., Ng, H., and Chen, N., "Aircraft Trajectory Optimization and Contrails Avoidance in the Presence of Winds," *Journal of Guidance, Control, and Dynamics* 34(5):1577-1584, 2011, https://doi.org/10.2514/1.53378.

35. Soler, M., Zou, B., and Hansen, M., "Flight Trajectory Design in the Presence of Contrails: Application of a Multiphase Mixed-Integer Optimal Control Approach," *Transportation*

Research Part C: Emerging Technologies 48:172-194, 2014, http://doi.org/10.1016/j.trc.2014.08.009.

36. Murrieta-Mendoza, A. and Botez, R.M., "Lateral Navigation Optimization Considering Winds and Temperatures for Fixed Altitude Cruise Using the Dijkstra's Algorithm," in *International Mechanical Engineering Congress & Exposition*, Montreal, Canada, 2014.
37. Dicheva, S. and Bestaoui, Y., "Three-Dimensional A* Dynamic Mission Planning for an Airborne Launch Vehicle," *Journal of Aerospace Information Systems* 11(2):98-106, 2014, http://doi.org/10.2514/1.I010070.
38. Murrieta-Mendoza, A., Romain, C., and Botez, R.M., "Commercial Aircraft Lateral Flight Reference Trajectory Optimization," *20th IFAC Symposium on Automatic Control in Aerospace ACA 2016* 49(17):1-6, 2016, http://doi.org/10.1016/j.ifacol.2016.09.001.
39. Félix-Patrón, R.S., Kessaci, A., and Botez, R., "Horizontal Flight Trajectories Optimisation for Commercial Aircraft through a Flight Management System," *The Aeronautical Journal* 118(1210):20, 2014.
40. Murrieta Mendoza, A., Bunel, A., and Botez, R., "Aircraft Lateral Flight Optimization Using Artificial Bees Colony," in *International Conference on Air Transport INAIR 2015*, Amsterdam, the Netherlands, 2015.
41. Murrieta-Mendoza, A., Hamy, A., and Botez, R.M., "Lateral Reference Trajectory Algorithm Using Ant Colony Optimization," in *16th AIAA Aviation Technology, Integration, and Operations Conference*, American Institute of Aeronautics and Astronautics, Washington, DC, 2016.
42. Rippel, E., Bar-Gill, A., and Shimkin, N., "Fast Graph-Search Algorithms for General-Aviation Flight Trajectory Generation," *Journal of Guidance, Control, and Dynamics* 28(4):801-811, 2005, http://doi.org/10.2514/1.7370.
43. Ng, H.K., Sridhar, B., and Grabbe, S., "Optimizing Aircraft Trajectories with Multiple Cruise Altitudes in the Presence of Winds," *Journal of Aerospace Information Systems* 11(1):35-47, 2014, http://doi.org/10.2514/1.I010084.
44. Félix-Patrón, R.S., Berrou, Y., and Botez, R.M., "New Methods of Optimization of the Flight Profiles for Performance Database-Modeled Aircraft," *Proceedings of the Institution of Mechanical Engineers, Part G: Journal of Aerospace Engineering* 1853-1867, 229, 2014, https://doi.org/10.1177/0954410014561772.
45. Félix-Patrón, R.S. and Botez, R.M., "Flight Trajectory Optimization Through Genetic Algorithms for Lateral and Vertical Integrated Navigation," *Journal of Aerospace Information Systems* 12(8):533-544, 2015, http://doi.org/10.2514/1.I010348.
46. Murrieta Mendoza, A., Mugnier, P., and Botez, R.M., "Vertical and Horizontal Flight Reference Trajectory Optimization for a Commercial Aircraft," in *Sci-Tech 2017 AIAA Guidance, Navigation, and Control Conference*, Grapevine, TX, 2017.
47. Zhou, Q.L., Zhang, Y., Qu, Y.H., and Rabbath, C.A., "Dead Reckoning and Kalman Filter design for Trajectory Tracking of a Quadrotor UAV," in *Proceedings of 2010 IEEE/ASME International Conference on Mechatronic and Embedded Systems and Applications*, Qingdao, China, 2010, 119-124.
48. Chen, Y., Yu, J., Mei, Y., Zhang, S. et al., "Trajectory Optimization of Multiple Quad-Rotor UAVs in Collaborative Assembling Task," *Chinese Journal of Aeronautics* 29(1):184-201, 2016, http://doi.org/10.1016/j.cja.2015.12.008.
49. Ghamry, K.A. and Zhang, Y., "Cooperative Control of Multiple UAVs for Forest Fire Monitoring and Detection," in *2016 12th IEEE/ASME International Conference on Mechatronic and Embedded Systems and Applications (MESA)*, Auckland, 2016, 1-6.
50. Liden, S., "Optimum 4D Guidance for Long Flights," in *11th IEEE/AIAA Digital Avionics Systems Conference, 1992*, Seattle, WA, 1992, 262-267.
51. Hagelauer, P. and Mora-Camino, F., "A Soft Dynamic Programming Approach for On-Line Aircraft 4D-Trajectory Optimization," *European Journal of Operational Research* 107(1):87-95, 1998, http://doi.org/10.1016/S0377-2217(97)00221-X.
52. Miyazawa, Y., Wickramasinghe, N.K., Harada, A., and Miyamoto, Y., "Dynamic Programming Application to Airliner Four Dimensional Optimal Flight Trajectory," in

AIAA Guidance, Navigation, and Control (GNC) Conference, American Institute of Aeronautics and Astronautics, Boston, MA, 2013.

53. Murrieta-Mendoza, A., Hamy, A., and Botez, R.M., "Mach Number Selection for Cruise Phase using the Ant Colony Optimization Algorithm With RTA Constrains," in *International Conference on Air Transport*, Amsterdam, the Netherlands, 2015.
54. Murrieta-Mendoza, A., Bunel, A., and Botez, R.M., "Aircraft Vertical Reference Trajectory Optimization with a RTA Constraint Using the ABC Algorithm," in *16th AIAA Aviation Technology, Integration, and Operations Conference*, American Institute of Aeronautics and Astronautics, Washington, DC, 2016.
55. Weibin Dai, J.Z., Delahaye, D., and Sun, X., "A Heuristic Algorithm for Aircraft 4D Trajectory Optimization Based on Bezier Curve," in *13th USA/Europe ATM R&D Seminar*, Vienna, AT, 2019, 10.
56. Ramasamy, S., Sabatini, R., Gardi, A.G., and Liu, Y., "Novel Flight Management System for Real-Time 4-Dimensional Trajectory Based Operations," in *AIAA Guidance, Navigation, and Control (GNC) Conference*, American Institute of Aeronautics and Astronautics, Boston, MA, 2013.
57. Gardi, A., Sabatini, R., Kistan, T., Lim, Y. et al., "4 Dimensional Trajectory Functionalities for Air Traffic Management Systems," in *2015 Integrated Communication, Navigation and Surveillance Conference (ICNS)*, Herdon, VA, 2015, N3-1-N3-11.
58. Gardi, A., Sabatini, R., and Ramasamy, S., "Multi-Objective Optimisation of Aircraft Flight Trajectories in the ATM and Avionics Context," *Progress in Aerospace Sciences* 83:1-36, 2016, http://doi.org/10.1016/j.paerosci.2015.11.006.
59. Murrieta-Mendoza, A., Ruiz, H., Kessaci, S., and Botez, R.M., "3D Reference Trajectory Optimization Using Particle Swarm Optimization," in in *17th AIAA Aviation Technology, Integration, and Operations Conference*, American Institute of Aeronautics and Astronautics, Denver, USA, 2017.
60. Murrieta-Mendoza, A., Ruiz, H., and Mihaela Botez, R., "Horizontal Flight Trajectory Optimization Considering RTA Constraints," *MATEC Web Conf.* 314:02002, 2020, https://doi.org/10.1051/matecconf/20203140200.
61. Kennedy, J. and Eberhart, R., "Particle Swarm Optimization," in *Neural Networks, 1995, Proceedings of ICNN'95 - International Conference on Neural Networks*, Perth, WA, Australia, Vol. 4, 1995, 1942-1948.
62. Robinson, M. and Kamine, S., "User Preference and Trajectory Options Sets (TOS) to Benefit Traffic Flow Management," in *AIAA Aviation 2019 Forum*, American Institute of Aeronautics and Astronautics, Dallas, Texas, 2019.
63. Cruciol, L., Clarke, J., and Weigang, L., "Trajectory Option Set Planning Optimization under Uncertainty in CTOP," in *2015 IEEE 18th International Conference on Intelligent Transportation Systems*, Las Palmas, 2015, 2084-2089.
64. Murrieta-Mendoza, A., and Botez, R.M., "Methodology for Vertical-Navigation Flight-Trajectory Cost Calculation Using a Performance Database," *Journal of Aerospace Information Systems* 12(8):519-532, 2015, http://doi.org/10.2514/1.I010347.
65. du Puy de Goyne, T., Plays, Y., Lepourry, P., and Besse, J., *Initiation à l'aéronautique* (Toulouse, France: Cépaduès - Éditions, 1995).
66. Ojha, S.K., "Optimization of Cruising Flights of Turbojet Aircraft," in *Flight Performance of Aircraft*, American Institute of Aeronautics and Astronautics, 1995, 237-258, ISBN: 978-1-56347-113-1, https://doi.org/10.2514/4.861826.